

UMAAF: UNVEILING AESTHETICS VIA MULTIFARIOUS ATTRIBUTES OF IMAGES

Wei jie Li^{1,*}, Yitian Wan^{1,*}, Xingjiao Wu^{2,†}, Junjie Xu¹, Cheng Jin², Liang He¹

¹East China Normal University, Shanghai, China

²Fudan University, Shanghai, China

ABSTRACT

With the increasing prevalence of smartphones and websites, Image Aesthetic Assessment (IAA) has become increasingly crucial. While the significance of attributes in IAA is widely recognized, many attribute-based methods lack consideration for the selection and utilization of aesthetic attributes. Our initial step involves the acquisition of aesthetic attributes from both intra- and inter-perspectives. Within the intra-perspective, we extract the direct visual attributes of images, constituting the absolute attribute. In the inter-perspective, our focus lies in modeling the relative score relationships between images within the same sequence, forming the relative attribute. Then, to better utilize image attributes in aesthetic assessment, we propose the Unified Multi-attribute Aesthetic Assessment Framework (UMAAF) to model both absolute and relative attributes of images. For absolute attributes, we leverage multiple absolute-attribute perception modules and a absolute-attribute interacting network. The absolute-attribute perception modules are first pre-trained on several absolute-attribute learning tasks and then used to extract corresponding absolute attribute features. The absolute-attribute interacting network adaptively learns the weight of diverse absolute-attribute features, effectively integrating them with generic aesthetic features from various absolute-attribute perspectives and generating the aesthetic prediction. To model the relative attribute of images, we consider the relative ranking and relative distance relationships between images in a Relative-Relation Loss function, which boosts the robustness of the UMAAF. Furthermore, UMAAF achieves the state-of-the-art performance on TAD66K and AVA datasets, and multiple experiments demonstrate the effectiveness of each module and the model’s alignment with human preference.

1. INTRODUCTION

Considering the incredibly ever-growing scale of visual data spreading online, Image Aesthetic Assessment (IAA) appears

* Wei jie Li and Yitian Wan contributed equally to this work. † Corresponding author: Xingjiao Wu (e-mail: xjwu.cs@fudan.edu.cn).



Fig. 1. Images with diverse aesthetic scores (1-10) and ‘GT’ denotes ground truth. The first row’s image scores are ranked high to low from left to right. Evaluators typically rate fig. 1(a) - fig. 1(c) first and then fig. 1(d), often resulting in a lower score due to its aesthetic difference compared to the other three images. The second row follows an opposing trend.

to be particularly significant for numerous downstream applications, such as image retrieval [1], photography [2], and image search [3]. Current research on aesthetic and psychology [4] have proved that any form of aesthetic experience comes down to a specific nervous system. Other studies [5, 6, 7] attempt to simulate the human aesthetic assessment process by modeling aesthetic attributes of the image itself have got remarkable results.

Although previous studies have demonstrated the efficacy of image attributes in facilitating the completion of IAA tasks is crucial, there are still two limitations. On the one hand, for attributes extracted from the image itself, they exhibit a lack of comprehensiveness [7, 6, 5, 8]. For example, the attribute like ‘rule-of-third’ is a common attribute used in previous studies, but it is only a part of the image composition. Besides, there is still room for exploration in the utilization of these extracted attributes. On the other hand, psychological research [9] suggests that the relative comparison between images can affect the results of aesthetic assessment, which is ignored by previous studies.

To alleviate the aforementioned challenges, we propose to extract the aesthetic attributes from intra- and inter-

perspectives of images. For the attributes extracted from the intra-perspective of images, specific elements such as composition, theme, and color play a direct and significant role in shaping the final aesthetic judgment made by individuals. For example, as illustrated in fig. 1 (c), the composition of an image contributes to the perceived spatial relationship between the primary subject and the background. When combined with other inherent attributes of the image, this composition leads to a visually pleasing experience, resulting in a high aesthetic score. These essential components, exerting a direct impact on the visual experience of individuals, are denoted as ‘absolute attributes’.

For the attributes extracted from the inter-perspective of images, they mainly come from the comparison of the images’ aesthetics within the same sequence, which has been verified by psychological research [9] that they can influence people’s aesthetic judgments, leading to potentially cognitive biases. For example, the evaluation of images within two rows where the assessment progresses from left to right. In the case of assessing fig. 1 (d) and fig. 1 (h), the final images in their respective rows, evaluators tend to assign lower scores to fig. 1 (d) compared to a direct evaluation, while the opposite tends to happen for fig. 1 (h). This phenomenon underscores the importance of considering the order in which images are presented. In the context of models’ aesthetic assessment, a notable example occurs when the training data lacks shuffling. This oversight can result in models learning incorrect relational features, impairing their ability to accurately assess aesthetics. This type of factor, which relies on comparisons or the arrangement of data rather than being directly derived from individual images and indirectly influences human visual judgments of images, is indicated as the ‘relative attribute’.

To harness the complete potential of aesthetic evaluation, incorporating both the absolute and relative attributes of images, we introduce the Unified Multi-Attribute Aesthetic Assessment Framework (UMA AF). This innovative framework integrates novel models and advanced loss functions to enhance the overall assessment process.

To address the absolute attributes, we introduce a purpose-built network aimed at their extraction and fusion. Guided by classical principles in photography [10], we pinpoint four fundamental and comprehensive attributes: Composition, Color, Exposure, and Theme, forming the foundation for our novel feature extraction component. Distinct from conventional direct feature concatenation methods [6, 7], we introduce an absolute-attribute interacting network. This component effectively merges the features extracted from absolute attributes with the overall aesthetic feature obtained from a shared network. To achieve this, we fuse the features from attributes perspectives and leverage bilinear fusion technique [11] within the fusion module, ultimately generating an aesthetic prediction score. In the realm of relative attributes, there has been a noticeable scarcity of IAA studies with a

dedicated focus on this aspect. To address the critical need for modeling the relative relationships among images, we devise an innovative loss function named the Relative-Relation Loss, which is implemented within the framework of triplet loss [12]. The Relative-Relation Loss captures the intricate interplay between images by considering both their relative rankings and the distance relationships.

In a nutshell, our main contributions are summarized as follows:

- **Unified Multi-Attribute Aesthetic Assessment Framework (UMA AF):** We introduce a comprehensive framework that takes both absolute and relative attributes of images into account. This framework incorporates multiple components, where each component is designed to handle a specific aspect of the image aesthetics. Additionally, we propose a novel loss function to capture the relative attribute information, enabling a more comprehensive perspective in learning the IAA task.
- **Efficient Extraction of Absolute Attributes:** We efficiently extract concrete absolute-attribute features from images, following real photographic rules. This is achieved through the deployment of multiple Absolute-Attribute Perception Components, where each component is designed to capture a specific absolute attribute. We ensure a comprehensive integration of these extracted features through our Absolute-Attribute Interacting Network, providing a holistic view.
- **Modeling Relative Attribute Information:** To effectively capture the relative attribute information between images, we introduce the Relative-Relation Loss. This loss function takes both the relative rankings and distance relationships between images into consideration, enhancing the model’s ability to perceive the aesthetic differences between images.
- **Empirical Performance and Alignment with Human Preference:** Through extensive experiments, we showcase that our model not only achieves state-of-the-art performance on aesthetic datasets but also closely aligns with human preference. Furthermore, our additional experiments validate the effectiveness of each component within our proposed model.

2. RELATED WORK

2.1. Image Aesthetic Assessment Methods

IAA has seen decades of evolution. Initially, hand-crafted features were used to represent image aesthetics [13, 14, 15, 16], but their limited capacity to handle diverse and complex images became evident. The emergence of deep learning revolutionized IAA, with researchers shifting to CNN or DNN-

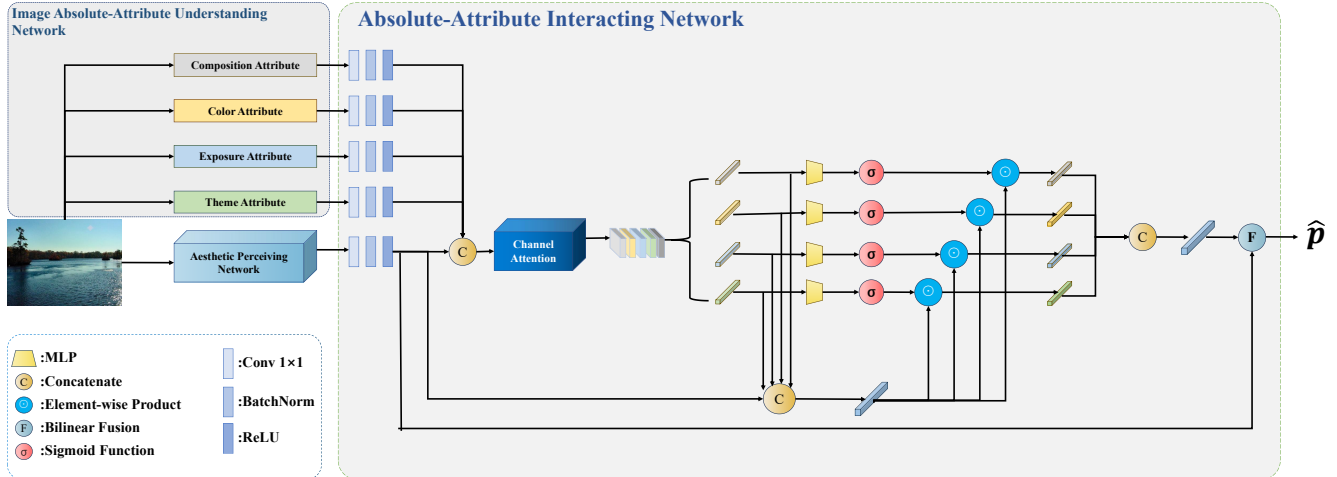


Fig. 2. Overview of the UMAAF. The whole architecture can be divided into three components: Image Absolute-Attribute Understanding Network, Absolute-Attribute Interacting Network and Aesthetic Perceiving Network. Image Absolute-Attribute Understanding Network has four branches used to extract corresponding attribute features, Absolute-Attribute Interacting Network adaptively fuses different features and Aesthetic Perceiving Network is mainly a MobileNetV2 network used to extract generic aesthetic features.

based approaches to learn aesthetic features, progressively replacing handcrafted ones. Early attempt like the RAPID model [17], was trained on IAA datasets, followed by methods such as DMA-Net [18] that used multiple patches in image training and A-Lamp [19] with a two-stream architecture for global and local features. NIMA [20] introduced an Earth Mover’s Distance loss for more accurate aesthetic score predictions, offering a distribution of scores rather than the simple binary classification.

A significant advancement is the introduction of the multi-level spatially pooled (MLSP) feature [21], derived from InceptionNet [22] convolution blocks, yielding more comprehensive image aesthetic representations. She *et al.* [23] used a multi-layer graph neural network to extract image composition information and achieves the best results in aesthetic classification tasks. Hou *et al.* [24] utilized object detection techniques to identify multiple objects within images, and then evaluate the image aesthetic based on the relation between objects. Pre-training strategies, such as adapting networks from image editing tasks [25] or expanding editing operations [26], led to notable improvements. However, these methods primarily focus on visual image features and often overlook the direct influence of image attributes on human perception. This aspect, which plays a crucial role in shaping human feelings toward images, is often neglected in these approaches.

2.2. Attribute-aware Aesthetic Assessment

As the importance of attributes in shaping human perception of image aesthetics became evident, attribute-aware approaches emerged. The SANE [7] employed pre-trained

deep networks to detect objects and extract scene information, which is then combined with aesthetic features. Celona *et al.* [8] focused on abstract attributes like composition and style, utilizing a hypernet to assess image aesthetics based on these extracted attributes. Adversarial learning is used in [27] to incorporate attributes like lights and the rule of thirds, and a multi-task deep network predicts both aesthetic scores and attributes, distinguished by a discriminator. Li *et al.* [5] involved pre-training tasks for multiple attributes, then using graph neural network to fuse different features. He *et al.* [28] delved into the significance of color in images for their aesthetic appeal. Notably, TANet [6] emphasized theme attributes, using a dedicated network to extract different theme rules from diverse images.

Compared to prior attribute-aware methods, our approach advances by extracting and modeling absolute and relative attributes simultaneously. For absolute attributes, our selection is based on pragmatic and comprehensive considerations. Furthermore, diverging from previous methodologies that placed lesser emphasis on integrating attribute features, we aim to investigate innovative techniques for combining these features. In the realm of relative attributes, a previously unexplored dimension, we introduce a loss function to capture inter-image relative relationships. This enriches the model’s understanding of aesthetic considerations within specific contextual settings.

3. FRAMEWORK

In this section, we will start by introducing our overall framework. Then, we will separately present the Image Absolute-Attribute Understanding Network and the Absolute-Attribute

Interacting Network. Finally, we will provide a detailed explanation of the Relative-Relation Loss.

3.1. Method

The architecture of the UMAAF is shown in fig. 2. The network architecture is specifically divided into three modules: 1) Image Absolute-Attribute Understanding Network: It extracts features that are relevant to determine absolute attributes from the image. 2) Aesthetic Perceiving Network: It mainly consists of a MobileNetV2 [29] and generates the generic aesthetic feature. 3) Absolute-Attribute Interacting Network: It interacts with the feature of each attribute and outputs the aesthetic prediction.

3.2. Absolute-Attribute Understanding Network

Inspired by classical rules of photography [10], we begin by identifying the absolute attributes to be perceived: Composition, Color, Exposure, and Theme. For the first three attributes, we employ three pre-trained Absolute-Attribute Perception Components, while the theme features are extracted by using a mature method from previous works [6, 7, 5].

The architecture of the Absolute-Attribute Perception Component is illustrated in fig. 3. Following the approach from [21], we use InceptionResNet-v2 [22] as the backbone, leveraging the multi-level features of the image. The component is divided into two parts: one utilizes a stack of convolution layers with various kernel sizes to focus on long-range information in image features through a larger receptive field, while the other part diversely aggregates and retains information using both the Average Pooling layer and Max Pooling layer.

We subsequently apply corresponding output layers and loss functions based on the specific pre-trained tasks. Next, we introduce the pre-training tasks of each absolute-attribute extractor.

Composition Attribute. Image composition quality is a crucial factor in assessing the aesthetic appeal of an image. We train our Attribute Perception Component on the CADB dataset [30], which serves as an image composition attribute extractor. The CADB dataset, comprising 9,958 real-world images, provides composition quality scores ranging from 1 to 5, where higher scores indicate better composition quality. It’s noteworthy that our attribute perception component, trained on the official partition of CADB, achieves remarkable results on its test set, with a PLCC (Pearson Linear Correlation Coefficient) of 0.715 and a SRCC (Spearman Rank Correlation Coefficient) of 0.705. These scores significantly outperform the state-of-the-art method on CADB as reported in the original paper [30] (PLCC: 0.671, SRCC: 0.656). This underscores the effectiveness of our Absolute-Attribute Perception Component in extracting image attributes, particularly in the context of image composition, validating the efficiency of our composition attribute extraction component.

Color Attribute. The image’s color significantly impacts its visual appeal. Vibrant colors often enrich the visual experience, while subdued colors with unique compositions or themes can evoke distinct emotions. To quantify this, we adopt the colorfulness classification method from [31], categorizing each image in the AVA dataset into 7 colorfulness levels: not colorful, slightly colorful, moderately colorful, averagely colorful, quite colorful, highly colorful, and extremely colorful. Besides, we pre-train an Absolute-Attribute Perception Component for the image color richness classification task. This enables the component to focus on regions of the image related to color, ultimately yielding a color feature extraction component.

Exposure Attribute. The exposure level of a photo, as highlighted in [32], significantly impacts its overall visual experience. Overexposure can make an image too bright, while underexposure can render it too dark, leading to distinct lighting conditions. We employ the dataset from [32] for pre-training, categorizing images into 5 exposure value (EV) categories. By conducting this pre-training task to classify exposure values, our model effectively focuses on the variations in light and shadow within the image. Consequently, we obtain an exposure and light feature extraction component.

Theme Attribute. Recent studies [6, 5] highlight the significant correlation between the theme of an image and its overall aesthetics. Inspired by the approach in TANet [6], we employ a pre-trained ResNet18 [33] model, trained on the Places dataset [34], as the image theme attribute extractor. The Places dataset comprises approximately 10 million images, covering over 400 distinct scene label categories. We utilize this branch to more effectively extract theme-related information from the image.

3.3. Absolute-Attribute Interacting Network

Most current IAA methods lack in-depth exploration of attribute fusion techniques. To address this, we introduce an Absolute-Attribute Interacting Network to fully utilize various attribute features.

Recognizing that different absolute attributes hold varying levels of importance for the final result on a single image, we employ the channel attention mechanism [35] to effectively weight these diverse absolute-attribute features. The input to the attention component is a concatenation of the aesthetic features and all absolute-attribute features, allowing us to leverage the image’s features fully. The attention component utilizes Max Pooling and Average Pooling to capture different context information and a shared parameter Multilayer Perceptron (MLP) to compute the ultimate attention weights.

After that, we get out the corresponding absolute-attribute features from the concatenation and transform them into feature vectors by an Average Pooling Layer. Then, inspired by [11], we use a feature selection mechanism to further integrate the absolute-attribute and aesthetic features from dif-

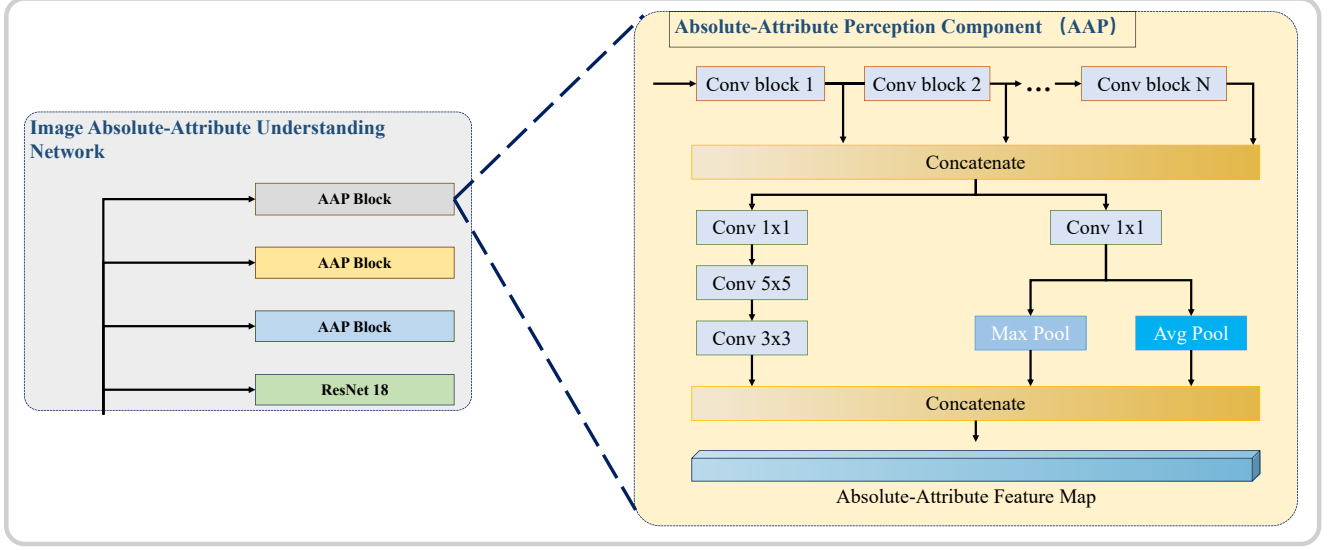


Fig. 3. The architecture of Absolute-Attribute Perception Component.

ferent attribute perspectives. Specifically, for each absolute attribute, we use a gate component to get attribute-specific features. The whole process can be described as follows:

$$z_i = \sigma(MLP_i(x_i)) \odot o, i \in \mathbf{S}, \quad (1)$$

where \mathbf{S} denotes the absolute-attributes set, including the absolute attributes determined before, x_i denotes the absolute-attribute feature vectors and o denotes the concatenation of all features. We do element-wise products using weights and concatenation of all features to get multiple attribute-specific features z_i .

Finally, we concatenate all attribute-specific features and use the bilinear fusion [11] to integrate them with generic aesthetic features and get the prediction.

3.4. Relative-Relation Loss

Current aesthetic evaluation methods [20, 36] pay more attention to modeling the features of the image itself, and the relation between images is rarely emphasized. Due to the importance of the relation of images in IAA, we develop Relative-Relation Loss to model the relative attributes of images and because of the feasibility, our loss function considers the samples in the same batch. As for the loss, first, consider i, j, k represent three samples in one batch, and their ground truth label is g_i, g_j, g_k , while meeting the condition that $g_i > g_j > g_k$ or $g_i < g_j < g_k$. We use sample i as the anchor and sample j, k as the positive and the negative one respectively. A triplet loss [12] is used to perform the following calculation:

$$L_{trp}(i, j, k) = \max\{0, |p_i - p_j| - |p_i - p_k| + |g_j - g_k|\}, \quad (2)$$

where p_i, p_j, p_k are the predicted values of three samples.

The introduced triplet loss function aims to increase the gap between the predicted scores of the anchor sample and the negative sample, while decreasing the gap between the anchor sample and the positive sample's predicted scores. The objective is to align these predicted scores' distances more closely with the distances between the ground truth. As such, the margin for the triplet loss is established as $|g_j - g_k|$, calculated based on a hypothetically perfect prediction environment [37].

Based on the triplet loss, considering the relationship between the sample and the other samples in the same batch, the Relative-Relation Loss can be formulated as follows:

$$L_{relative} = \frac{1}{b-4} \sum_{i=3}^{b-2} \left(\frac{1}{b-3} \left(\sum_{j=2}^{i-1} L_{trp}(i, j, j-1) + \sum_{j=i+1}^{b-1} L_{trp}(i, j, j+1) \right) \right), \quad (3)$$

where b means the batch size. When training, we sort the samples in one batch by ground truth labels from the largest to the smallest firstly. Then, samples in the same batch are used as anchors in turn, and other neighboring samples are selected as positive samples and negative samples in pairs.

We utilize the loss as defined in eq. (4) to constrain the UMAAF:

$$L_{total} = L(\hat{p}, p) + \lambda L_{relative}, \quad (4)$$

where λ is the balancing coefficient and set to 0.05 during training. \hat{p} and p represent the output of the model and the label respectively. The $L(i, j)$ is the Earth Mover's Distance(EMD) [20] loss if the label is the aesthetic distribution

or Mean Squared Error(MSE) loss when the label is aesthetic score.

4. EXPERIMENTS

In this section, we will first describe the experimental setup for the pre-training phase and the overall training phase. Subsequently, we compare UMAAF with the state-of-the-art methods on the aesthetic datasets: AVA [45] and TAD66K [6]. Following the previous methods [20, 21], we use PLCC, SRCC and Accuracy to evaluate the results. In addition, the MSE loss and EMD loss on test set [6] are also included in the evaluation metrics of TAD66K[6] and AVA [45] respectively. Finally, we perform ablation experiments to verify the validity of each component and selected attributes.

4.1. Implementation Details

Pre-training Settings. During the pre-training phase, we utilize a pre-trained InceptionResNet-v2 [22] from ImageNet [46] as the backbone for our Absolute-Attribute Perception Components. Each image used for pre-training is initially resized to $330 \times 330 \times 3$ and subsequently randomly cropped to $299 \times 299 \times 3$ for input. We employ an Adam optimizer with a batch size of 32 and apply a weight decay of $5e^{-4}$. The initial learning rate is set to $1e^{-4}$.

Training Settings. During training, we keep the pre-trained feature extractors' parameters frozen. Images are resized to $224 \times 224 \times 3$ for the backbone and theme attribute extractor and $299 \times 299 \times 3$ for the other attribute extractors. Random horizontal flipping is used for data augmentation. We utilize the Adam optimizer with a batch size of 32, weight decay of $5e^{-4}$, and an initial learning rate of $1e^{-6}$. If the network's loss doesn't decrease for 5 consecutive epochs, we reduce the learning rate by a factor of 0.1. Training stops when the loss ceases to decrease. The network is implemented in PyTorch and runs on an A100 GPU with 40GB memory.

4.2. Performance Comparison

The results of the proposed model and the comparison with other known methods are shown in table 1.

Performance on TAD66K Dataset. On the TAD66K dataset, UMAAF achieves state-of-the-art performance on all metrics. Compared with the previous work [6], UMAAF further models more absolute attributes in the network and different from directly concatenating multiple features, we further integrate various features from a more comprehensive perspective. The comparison results show the promotion from effective utilization of absolute attributes.

Performance on AVA Dataset. We outperform other methods in all metrics except SRCC and Accuracy. Among them, SRCC is close to the current best result and still competitive. Compared to previous works which mostly develop

information within the images themselves, we additionally model the relative information between images and obtain a higher PLCC and significantly lower EMD value.

Performance on human preference. We employ ImageReward [47] to assess the model's compliance with human preference. ImageReward is used to evaluate the degree of human preference for text-to-image results. Giving a piece of text and an image to the model, it will return the score that reflects the image's degree of human preference. We use a text: ' a photograph of high aesthetic quality, with variable and real content ' to describe the images in the aesthetic dataset as the text input of ImageReward and combine it with the images in the dataset to get the model's assessment. We normalize the human preference score obtained by ImageReward and the aesthetic score obtained by the model, and then calculated the PLCC and SRCC between them to evaluate the correlation between the models' results and human preference. We selected NIMA [20], MLSP [21], TANet [6] and UMAAF to compare, and the results are shown in table 2. The results prove that UMAAF is more consistent with human preference than other representative aesthetic assessment models.

4.3. Ablation Study

Effectiveness of modules and loss function. table 3 summarizes the outcomes of our ablation study conducted on the TAD66K dataset [6]. Initially, we evaluate the impact of the loss function when applied solely to the backbone. The introduction of this loss function leads to a 3.3% increase in PLCC and a 1.4% increase in SRCC for the model.

Next, each absolute-attribute branch is individually added to the backbone to assess their effectiveness. Notably, the composition and theme branches exhibit the most significant improvements. Upon integrating the composition branches, PLCC and SRCC rise by 6.3% and 6.4% respectively, underscoring the importance of composition and theme in image aesthetics assessment. This reaffirms that absolute-attribute features aid the network in gaining a better understanding of image aesthetics.

Once all attributes are incorporated, we delve into the effects of the loss function and the Absolute-Attribute Interacting Network. When added to models that already possess all attribute branches, the proposed loss function results in a 1.7% increase in PLCC and a 1.5% increase in SRCC. Moreover, the attribute fusion component yields a 2.2% increase in PLCC and a 1.8% increase in SRCC. These findings validate the effectiveness of the Absolute-Attribute Interacting Network in enhancing the fusion of absolute-attribute features and aesthetic features from the image, leading to more substantial improvements. Additionally, modeling relative attributes of images effectively enhances the overall results.

Effectiveness of extracting absolute-attributes with different structures. As shown in table 4, we tested the effectiveness of extracting absolute-attribute features with differ-

Table 1. Comparison of the proposed model with the state-of-the-art IAA methods on TAD66K and AVA. '-' means the results are not available in known papers. The results on TAD66K are mainly from [6] and the results on AVA are from respective papers.

Method	TAD66K			AVA			
	PLCC \uparrow	SRCC \uparrow	MSE \downarrow	PLCC \uparrow	SRCC \uparrow	Accuracy \uparrow	EMD \downarrow
RAPID [17]	0.332	0.314	0.022	0.453	0.447	71.18	-
ALamp [19]	0.422	0.411	0.019	0.671	0.666	82.52	-
NIMA [20]	0.405	0.390	0.021	0.636	0.612	81.49	0.05
MPada [38]	0.480	0.466	0.022	0.731	0.727	83.03	-
MLSP [21]	0.508	0.490	0.019	0.757	0.756	81.72	-
UIAA [39]	0.441	0.433	0.021	0.720	0.719	80.79	0.065
GPF-CNN [40]	-	-	-	0.704	0.690	81.81	-
AFDC [41]	-	-	-	0.671	0.649	83.18	-
ReLIC [42]	-	-	-	0.760	0.748	82.35	-
Xu <i>et al.</i> [43]	-	-	-	0.725	0.724	80.9	-
Hou <i>et al.</i> [24]	-	-	-	0.753	0.751	81.67	-
HGCN [23]	0.493	0.486	0.020	0.687	0.665	84.61	0.043
MUSIQ [44]	-	-	-	0.738	0.726	81.5	-
TANet [6]	0.531	0.513	0.016	0.765	0.758	80.63	0.047
GAT-GATP [36]	-	-	-	0.764	0.762	-	-
TAVAR [5]	-	-	-	0.736	0.725	-	-
UMAAF	0.540	0.515	0.015	0.770	0.759	81.69	0.042

Table 2. Comparison of the proposed model with several representative IAA methods on human preference.

Method	PLCC \uparrow	SRCC \uparrow
NIMA [20]	0.234	0.231
MLSP [21]	0.246	0.241
TANet [6]	0.249	0.250
UMAAF	0.261	0.254

ent structures, mainly focusing on pre-training tasks for attributes such as composition, color, and exposure. We first directly used multiple classic CNN models for testing, and the experimental results demonstrated better extraction of absolute image attributes is beneficial for improving the final aesthetic evaluation. Afterward, we use the combination of features from each layer in InceptionResNetv2 for attribute extraction tasks. The "w/o cnn" and "w/o pool" separately denote that just use the branch with pooling layers and the branch with convolution layers in Absolute-Attribute Perception(AAP). The experimental results demonstrate that AAP which uses both convolution and combined pooling layers simultaneously can fully utilize the extracted features.

Effectiveness of absolute-attribute selection. We further test the effects of the selected absolute attributes. Following the approach of other papers [5, 27], we use multiple identical Absolute-Attribute Perception Components to learn

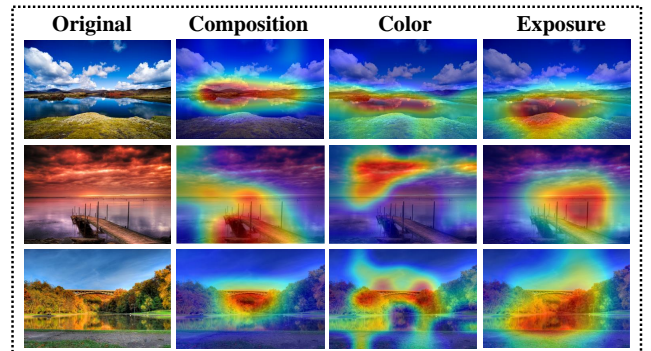


Fig. 4. Qualitative analysis results for each attribute branch. It shows that each attribute branches focus on the regions of the image that can reflect the attribute characteristics.

each absolute attribute of the image from the AADB dataset [48]: 'Balancing Element', 'Color Harmony', 'Interesting Content', 'Shallow DOF', 'Good Lighting', 'Rule of Thirds', 'Vivid Color'. table 5 shows the relatively better results of learning every single attribute on the AADB and the effects of the overall model on the TAD66K dataset after branching each absolute attribute into it. It indicates that although these absolute attributes can effectively promote the aesthetic evaluation task, selecting correct image absolute attributes and using more data to learn the attribute features can achieve better results.

Table 3. Ablation study results on TAD66K.

PLCC	SRCC	MobileNetV2	Composition Attribute	Color Attribute	Exposure Attribute	Theme Attribute	Relative Loss	Attribute Interaction
0.456	0.447	✓						
0.471	0.453	✓					✓	
0.485	0.475	✓	✓					
0.473	0.467	✓		✓				
0.478	0.477	✓			✓			
0.481	0.471	✓				✓		
0.505	0.482	✓	✓			✓		
0.502	0.487	✓	✓	✓	✓			
0.513	0.489	✓	✓	✓	✓	✓		
0.522	0.497	✓	✓	✓	✓	✓	✓	
0.524	0.498	✓	✓	✓	✓	✓		✓
0.540	0.515	✓	✓	✓	✓	✓	✓	✓

Table 4. Results of different structures on extracting multi absolute attributes and the corresponding final results on TAD66K.

Models	Composition		Color	Exposure	TAD66K	
	PLCC ↑	SRCC ↑	Accuracy ↑	Accuracy ↑	PLCC ↑	SRCC ↑
ResNet18	0.597	0.586	85.64%	84.11%	0.515	0.490
ResNet34	0.613	0.603	86.60%	84.96%	0.518	0.492
ResNet50	0.622	0.612	88.69%	87.06%	0.522	0.496
InceptionResNetv2	0.642	0.634	88.98%	88.34%	0.522	0.501
AAP (w/o cnn)	0.695	0.685	0.40%	89.03%	0.532	0.508
AAP (w/o pool)	0.688	0.667	89.44%	88.51%	0.524	0.505
AAP	0.715	0.705	90.82%	89.84%	0.540	0.515

Table 5. Results of learning partial attributes on the AADB dataset and effect on the TAD66k after branching attributes into the model.

Metrics	Color Harmony	Shallow DoF	Good Lighting	Interesting Content	Rule of Thirds	Vivid Color	All Attribute on TAD66K
PLCC	0.459	0.716	0.501	0.566	0.244	0.706	0.519
SRCC	0.453	0.492	0.433	0.564	0.236	0.699	0.494

4.4. Model Interpretation

Class Activation Maps. We employed Layer Class Activation Mapping (Layer-CAM) [49] to visualize feature maps for each absolute-attribute branch to highlight model focus areas, as shown in fig. 4, while Layer-CAM improves the accuracy of the generated heat map compared to basic CAM. The red areas indicate regions that the model prioritizes. As theme attributes have been extensively studied, our analysis primarily concentrates on composition, color, and exposure attributes. The visualization reveals that the composition and color branches focus on image regions relevant to their respective attributes. Additionally, the exposure branch emphasizes not only the dark and light areas but also regions related to light. These visualization outcomes affirm the effectiveness

of AAP.

Dynamic Fusion of Attribute Features. We label each image in the test set by clustering attention weight vectors generated in the Absolute-Attribute Interacting Network. The partial resulting labels are visualized using t-SNE transformation. Each image’s weight vector is depicted as a colored dot, and images sharing the same color belong to the same cluster, as seen in fig. 5. Notably, we observe that images with similar absolute attributes have weight vectors close to each other. For instance, images with blue dots share similar composition, theme, and exposure attributes, with relatively minor differences in color attributes. Additionally, images with red dots, despite differing themes, display close weight distributions due to similarities in other attributes. Considering aesthetic feature vectors during weight adjustment, the impact of

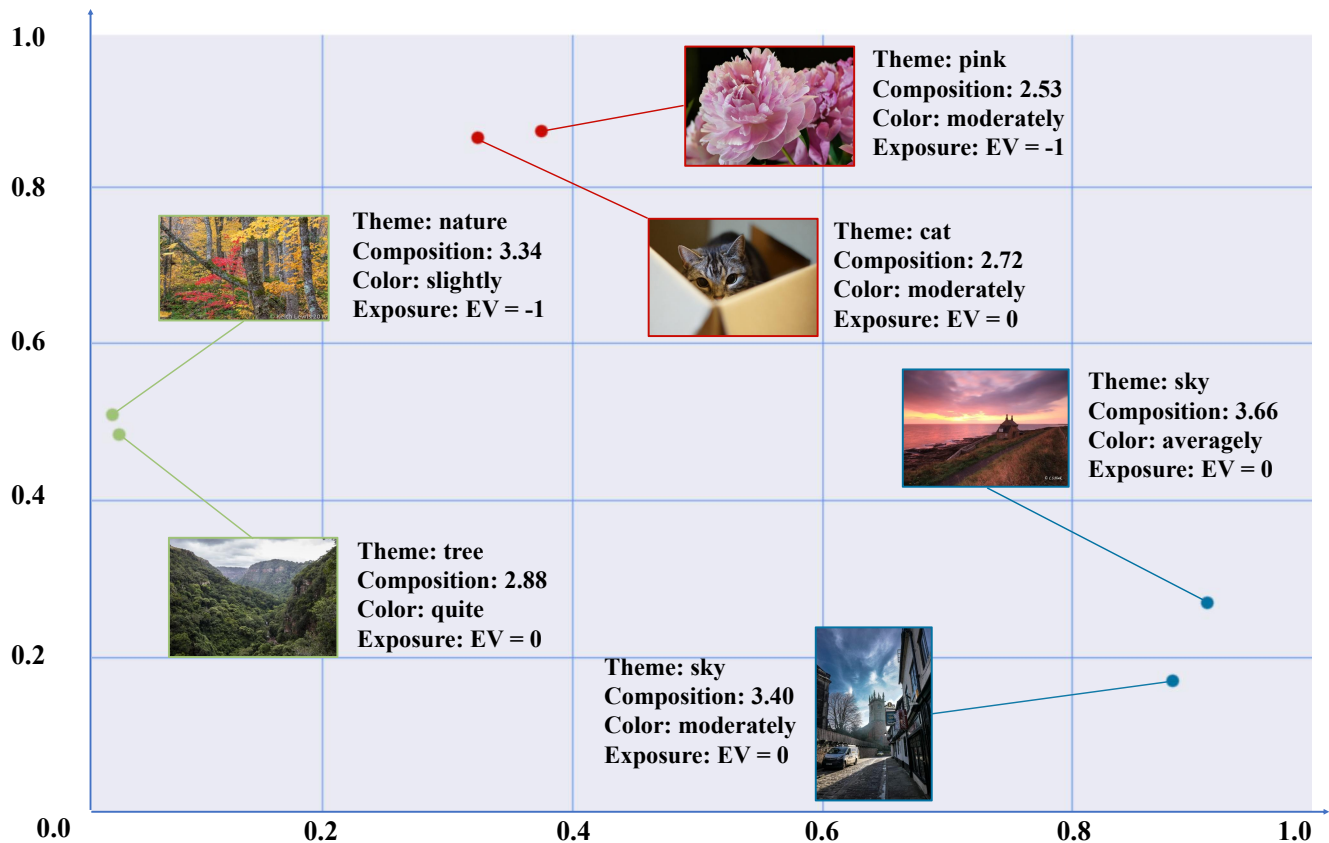


Fig. 5. The cluster of Absolute-Attribute Weights after t-SNE transformation of several images on TAD66K test set. The attributes of each image predicted are beside them.

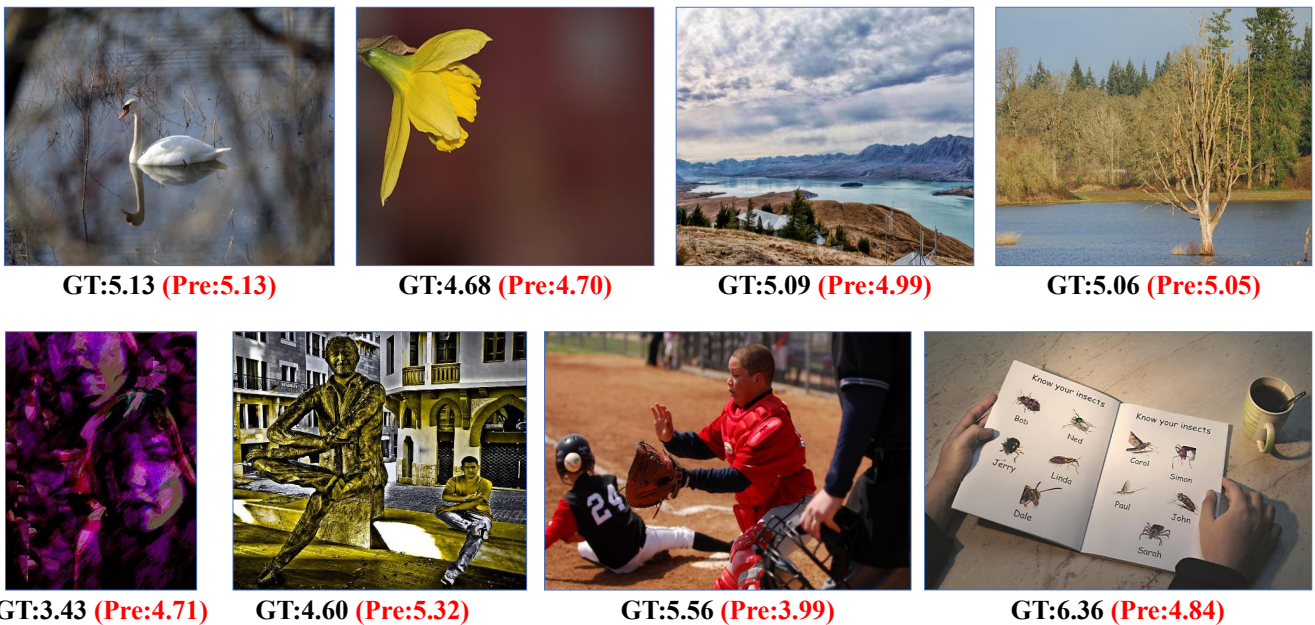


Fig. 6. UMAAF prediction results: successes (first row) and failures (second row). ‘GT’ and ‘Pre’ are the ground truth and prediction results of UMAAF, respectively.

each image’s unique features on overall weighting becomes evident. This leads to similar weighting for feature vectors in images with distinct attributes, as seen in green-framed images. This phenomenon further validates the self-adaptive nature of the module.

Prediction Results Analysis. We further analyze the success and failure prediction outcomes of UMAAF, as shown in fig. 6. The first row shows several successful cases and the second row shows several failure cases. In the first row, it shows that if the image has sufficiently distinct and explicit attributes, our predictions tend to be better. And if the aesthetic quality of the image is closely related to its semantic content, as shown in the second row, UMAAF understands these abstract semantics inadequately, resulting in significant prediction errors.

5. CONCLUSIONS

In this paper, we introduce UMAAF, a comprehensive framework that handles both absolute and relative attributes of images for IAA. We extract determined absolute attributes by the Absolute-Attribute Perception Component and propose an Absolute-Attribute Interacting Network that dynamically learns attribute weights, effectively integrating diverse absolute-attribute perspectives and generating aesthetic predictions. For modeling relative attributes, we introduce the Relative-Relation Loss, considering the relative rankings and distance relationships between images, further enhancing performance. Extensive experiments demonstrate our model’s state-of-the-art performance and its alignment with human preference. However, our approach still has limitations. There is still a significant unexplored territory in attribute selection and utilization for image aesthetic assessment. In future work, we intend to conduct further in-depth research in related areas to advance image aesthetic understanding.

6. REFERENCES

- [1] Fangcen Liu, Chenqiang Gao, Yongqing Sun, Yue Zhao, Feng Yang, Anyong Qin, and Deyu Meng, “Infrared and visible cross-modal image retrieval through shared features,” *IEEE Transactions on Circuits and Systems for Video Technology*, vol. 31, no. 11, pp. 4485–4496, 2021.
- [2] Yogesh Singh Rawat and Mohan S. Kankanhalli, “Clicksmart: A context-aware viewpoint recommendation system for mobile photography,” *IEEE Transactions on Circuits and Systems for Video Technology*, vol. 27, no. 1, pp. 149–158, 2017.
- [3] Yubin Deng, Chen Change Loy, and Xiaoou Tang, “Image aesthetic assessment: An experimental survey,” *IEEE Signal Processing Magazine*, vol. 34, no. 4, pp. 80–106, 2017.
- [4] John Dewey, “Art as experience,” in *The richness of art education*, pp. 33–48. 2008.
- [5] Leida Li, Yipo Huang, Jinjian Wu, Yuzhe Yang, Yaqian Li, Yandong Guo, and Guangming Shi, “Theme-aware visual attribute reasoning for image aesthetics assessment,” *IEEE Transactions on Circuits and Systems for Video Technology*, 2023.
- [6] Shuai He, Yongchang Zhang, Rui Xie, Dongxiang Jiang, and Anlong Ming, “Rethinking image aesthetics assessment: Models, datasets and benchmarks,” in *International Joint Conference on Artificial Intelligence (IJCAI)*, 2022, pp. 942–948.
- [7] Chaoran Cui, Huihui Liu, Tao Lian, Liqiang Nie, Lei Zhu, and Yilong Yin, “Distribution-oriented aesthetics assessment with semantic-aware hybrid network,” *IEEE transactions on multimedia*, vol. 21, no. 5, pp. 1209–1220, 2018.
- [8] Luigi Celona, Marco Leonardi, Paolo Napoletano, and Alessandro Rozza, “Composition and style attributes guided image aesthetic assessment,” *IEEE Transaction on Image Processing*, vol. 31, pp. 5009–5024, 2022.
- [9] Dan Ariely and Simon Jones, *Predictably irrational*, HarperCollins New York, 2008.
- [10] Bruce Barnbaum, *The art of photography: A personal approach to artistic expression*, Rocky Nook, Inc., 2017.
- [11] Kelong Mao, Jieming Zhu, Liangcai Su, Guohao Cai, Yuru Li, and Zhenhua Dong, “Finalmlp: An enhanced two-stream mlp model for ctr prediction,” in *The AAAI Conference on Artificial Intelligence (AAAI)*, 2023, vol. 37.
- [12] Florian Schroff, Dmitry Kalenichenko, and James Philbin, “Facenet: A unified embedding for face recognition and clustering,” in *Conference on Computer Vision and Pattern Recognition (CVPR)*, 2015, pp. 815–823.
- [13] Pere Obrador, Ludwig Schmidt-Hackenberg, and Nuria Oliver, “The role of image composition in image aesthetics,” in *IEEE International Conference on Image Processing (ICIP)*. IEEE, 2010, pp. 3185–3188.
- [14] Ritendra Datta, Dhiraj Joshi, Jia Li, and James Z Wang, “Studying aesthetics in photographic images using a computational approach,” in *European Conference on Computer Vision (ECCV)*, 2006, pp. 288–301.
- [15] Masashi Nishiyama, Takahiro Okabe, Imari Sato, and Yoichi Sato, “Aesthetic quality classification of photographs based on color harmony,” in *Conference*

- on *Computer Vision and Pattern Recognition (CVPR)*. IEEE, 2011, pp. 33–40.
- [16] Xiaoshuai Sun, Hongxun Yao, Rongrong Ji, and Shao-hui Liu, “Photo assessment based on computational visual attention model,” in *ACM International Conference on Multimedia (ACMMM)*, 2009, pp. 541–544.
- [17] Xin Lu, Zhe Lin, Hailin Jin, Jianchao Yang, and James Z Wang, “Rapid: Rating pictorial aesthetics using deep learning,” in *ACM International Conference on Multimedia (ACMMM)*, 2014, pp. 457–466.
- [18] Xin Lu, Zhe Lin, Xiaohui Shen, Radomir Mech, and James Z Wang, “Deep multi-patch aggregation network for image style, aesthetics, and quality estimation,” in *Conference on Computer Vision and Pattern Recognition (CVPR)*, 2015, pp. 990–998.
- [19] Shuang Ma, Jing Liu, and Chang Wen Chen, “A-lamp: Adaptive layout-aware multi-patch deep convolutional neural network for photo aesthetic assessment,” in *Conference on Computer Vision and Pattern Recognition (CVPR)*, 2017, pp. 4535–4544.
- [20] Hossein Talebi and Peyman Milanfar, “Nima: Neural image assessment,” *IEEE Transaction on Image Processing*, vol. 27, no. 8, pp. 3998–4011, 2018.
- [21] Vlad Hosu, Bastian Goldlucke, and Dietmar Saupe, “Effective aesthetics prediction with multi-level spatially pooled features,” in *Conference on Computer Vision and Pattern Recognition (CVPR)*, 2019, pp. 9375–9383.
- [22] Christian Szegedy, Sergey Ioffe, Vincent Vanhoucke, and Alexander Alemi, “Inception-v4, inception-resnet and the impact of residual connections on learning,” in *The AAAI Conference on Artificial Intelligence (AAAI)*, 2017, vol. 31.
- [23] Dongyu She, Yu-Kun Lai, Gaoxiong Yi, and Kun Xu, “Hierarchical layout-aware graph convolutional network for unified aesthetics assessment,” in *Conference on Computer Vision and Pattern Recognition (CVPR)*, 2021, pp. 8475–8484.
- [24] Jingwen Hou, Sheng Yang, and Weisi Lin, “Object-level attention for aesthetic rating distribution prediction,” in *ACM International Conference on Multimedia (ACMMM)*, 2020, pp. 816–824.
- [25] Kekai Sheng, Weiming Dong, Menglei Chai, Guohui Wang, Peng Zhou, Feiyue Huang, Bao-Gang Hu, Rongrong Ji, and Chongyang Ma, “Revisiting image aesthetic assessment via self-supervised feature learning,” in *The AAAI Conference on Artificial Intelligence (AAAI)*, 2020, vol. 34, pp. 5709–5716.
- [26] Ran Yi, Haoyuan Tian, Zhihao Gu, Yu-Kun Lai, and Paul L Rosin, “Towards artistic image aesthetics assessment: a large-scale dataset and a new method,” in *Conference on Computer Vision and Pattern Recognition (CVPR)*, 2023, pp. 22388–22397.
- [27] Bowen Pan, Shangfei Wang, and Qisheng Jiang, “Image aesthetic assessment assisted by attributes through adversarial learning,” in *The AAAI Conference on Artificial Intelligence (AAAI)*, 2019, vol. 33, pp. 679–686.
- [28] Shuai He, Anlong Ming, Yaqi Li, Jinyuan Sun, ShunTian Zheng, and Huadong Ma, “Thinking image color aesthetics assessment: Models, datasets and benchmarks,” in *International Conference on Computer Vision (ICCV)*, 2023, pp. 21838–21847.
- [29] Mark Sandler, Andrew Howard, Menglong Zhu, Andrey Zhmoginov, and Liang-Chieh Chen, “Mobilenetv2: Inverted residuals and linear bottlenecks,” in *Conference on Computer Vision and Pattern Recognition (CVPR)*, 2018, pp. 4510–4520.
- [30] Liqing Zhang Bo Zhang, Li Niu, “Image composition assessment with saliency-augmented multi-pattern pooling,” in *British Machine Vision Conference (BMVC)*, 2021.
- [31] David Hasler and Sabine E Suesstrunk, “Measuring colorfulness in natural images,” in *Human vision and electronic imaging VIII*, 2003, vol. 5007, pp. 87–95.
- [32] Mahmoud Afifi, Konstantinos G Derpanis, Bjorn Ommer, and Michael S Brown, “Learning multi-scale photo exposure correction,” in *Conference on Computer Vision and Pattern Recognition (CVPR)*, 2021, pp. 9157–9167.
- [33] Kaiming He, Xiangyu Zhang, Shaoqing Ren, and Jian Sun, “Deep residual learning for image recognition,” in *Conference on Computer Vision and Pattern Recognition (CVPR)*, 2016, pp. 770–778.
- [34] Bolei Zhou, Agata Lapedriza, Aditya Khosla, Aude Oliva, and Antonio Torralba, “Places: A 10 million image database for scene recognition,” *IEEE Transaction on Pattern Analysis and Machine Intelligence*, vol. 40, no. 6, pp. 1452–1464, 2017.
- [35] Sanghyun Woo, Jongchan Park, Joon-Young Lee, and In So Kweon, “Cbam: Convolutional block attention module,” in *European Conference on Computer Vision (ECCV)*, 2018, pp. 3–19.
- [36] Koustav Ghosal and Aljosa Smolic, “Image aesthetics assessment using graph attention network,” in *Proceedings of the International Conference on Pattern Recognition (ICPR)*, 2022, pp. 3160–3167.

- [37] S Alireza Golestaneh, Saba Dadsetan, and Kris M Kitani, “No-reference image quality assessment via transformers, relative ranking, and self-consistency,” in *IEEE Winter Conference on Applications of Computer Vision (WACV)*, 2022, pp. 1220–1230.
- [38] Kekai Sheng, Weiming Dong, Chongyang Ma, Xing Mei, Feiyue Huang, and Bao-Gang Hu, “Attention-based multi-patch aggregation for image aesthetic assessment,” in *ACM International Conference on Multimedia (ACMMM)*, 2018, pp. 879–886.
- [39] Huiyu Zeng, Zisheng Cao, Lei Zhang, and Alan Conrad Bovik, “A unified probabilistic formulation of image aesthetic assessment,” *IEEE Transaction on Image Processing*, vol. 29, pp. 1548–1561, 2020.
- [40] Xiaodan Zhang, Xinbo Gao, Wen Lu, and Lihuo He, “A gated peripheral-foveal convolutional neural network for unified image aesthetic prediction,” *IEEE Transactions on Multimedia*, vol. 21, no. 11, pp. 2815–2826, 2019.
- [41] Qiuyu Chen, Wei Zhang, Ning Zhou, Peng Lei, Yi Xu, Yu Zheng, and Jianping Fan, “Adaptive fractional dilated convolution network for image aesthetics assessment,” in *Conference on Computer Vision and Pattern Recognition (CVPR)*, 2020, pp. 14114–14123.
- [42] Lin Zhao, Meimei Shang, Fei Gao, Rongsheng Li, Fei Huang, and Jun Yu, “Representation learning of image composition for aesthetic prediction,” *Computer Vision and Image Understanding*, vol. 199, pp. 103024, 2020.
- [43] Munan Xu, Jia-Xing Zhong, Yurui Ren, Shan Liu, and Ge Li, “Context-aware attention network for predicting image aesthetic subjectivity,” in *ACM International Conference on Multimedia (ACMMM)*, 2020, pp. 798–806.
- [44] Junjie Ke, Qifei Wang, Yilin Wang, Peyman Milanfar, and Feng Yang, “Musiq: Multi-scale image quality transformer,” in *International Conference on Computer Vision (ICCV)*, 2021, pp. 5148–5157.
- [45] Naila Murray, Luca Marchesotti, and Florent Perronnin, “Ava: A large-scale database for aesthetic visual analysis,” in *Conference on Computer Vision and Pattern Recognition (CVPR)*, 2012, pp. 2408–2415.
- [46] Jia Deng, Wei Dong, Richard Socher, Li-Jia Li, Kai Li, and Li Fei-Fei, “Imagenet: A large-scale hierarchical image database,” in *Conference on Computer Vision and Pattern Recognition (CVPR)*, 2009, pp. 248–255.
- [47] Jiazheng Xu, Xiao Liu, Yuchen Wu, Yuxuan Tong, Qinkai Li, Ming Ding, Jie Tang, and Yuxiao Dong, “Imagereward: Learning and evaluating human preferences for text-to-image generation,” *arXiv preprint arXiv:2304.05977*, 2023.
- [48] Shu Kong, Xiaohui Shen, Zhe Lin, Radomir Mech, and Charless Fowlkes, “Photo aesthetics ranking network with attributes and content adaptation,” in *European Conference on Computer Vision (ECCV)*, 2016, pp. 662–679.
- [49] Peng-Tao Jiang, Chang-Bin Zhang, Qibin Hou, Ming-Ming Cheng, and Yunchao Wei, “Layercam: Exploring hierarchical class activation maps for localization,” *IEEE Transaction on Image Processing*, vol. 30, pp. 5875–5888, 2021.
- [50] Yuming Fang, Yan Zeng, Wenhui Jiang, Hanwei Zhu, and Jiebin Yan, “Superpixel-based quality assessment of multi-exposure image fusion for both static and dynamic scenes,” *IEEE Transaction on Image Processing*, vol. 30, pp. 2526–2537, 2021.

UMAAF: Unveiling Aesthetics via Multifarious Attributes of Images

Supplementary Material

This supplementary material will provide more description, experiment, and visualization results, and organized as outlined below:

- Section A: Extended samples and detailed insights into the absolute-attribute pre-training task. This section presents further samples and elaborates on the nuances of our absolute-attribute pre-training task.
- Section B: In-depth architecture of UMAAF and encompassed features. Detailed information is provided regarding the architecture of UMAAF and the various features it encompasses.
- Section C: Comprehensive experiments on the balancing coefficient of the Relative-Relation Loss and its derivation. This section expands on the experimentation involving the balancing coefficient of the Relative-Relation Loss. Furthermore, it offers a more detailed derivation process for this coefficient.
- Section D: Elaborate clarification of the dataset and utilized evaluation metrics. A thorough explanation of the dataset utilized in our study is provided in this section, along with a detailed overview of the evaluation metrics we have adopted.
- Section E: Extended visualized results and in-depth analysis. This section presents a broader range of visualized outcomes and delves deeper into the analysis of these results.
- Section F: We will present more details on the ablation experiment of AAP.
- Section G: Some examples of the impact of changing image attributes on image aesthetic scores.

A. MORE DETAILS OF PRE-TRAINING TASKS

We use Absolute-Attribute Perception Components to pre-train on datasets corresponding to three absolute attributes: composition, color, and exposure. Some samples of three datasets are shown in fig. A1. The details regarding the composition attribute pre-training task have already been explained in the main paper and for the color attribute, we get a 90.82% accuracy on the test set.

For the exposure attribute, we employ the dataset from [32] for pre-training. In order to facilitate better pre-training, we input correctly exposed images in the dataset along with the images that need to be classified. Due to the goal of directing the model’s attention to specific regions in the images

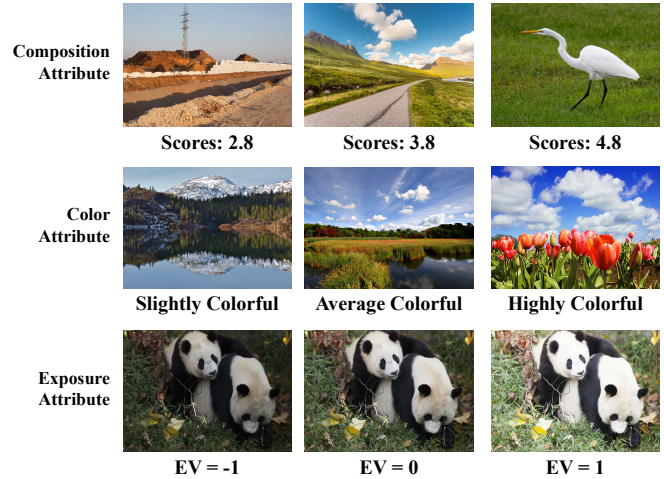


Fig. A1. Some samples of three pre-training tasks.

rather than achieving high classification scores, we use all images in the dataset to pre-train and get a 89.84% accuracy on the train set.

We adopt Mean Squared Error(MSE) loss for the pre-training task of composition attribute and Cross Entropy loss for the pre-training tasks of color and exposure attributes.

B. MORE DETAILS OF THE UMAAF

In Absolute-Attribute Perception Component, we first resize the feature maps via ‘area’ interpolate and concatenate the feature maps from multi Conv blocks into one feature map with the size of $16928 \times 7 \times 7$. Then, through the next two parts of the Absolute-Attribute Perception Component, we get two feature maps with the size of $1024 \times 7 \times 7$ respectively and concatenate them into one feature map with the size of $2048 \times 7 \times 7$, which is sent to Absolute-Attribute Interacting Network. The feature maps from the theme extractor and Aesthetics Perceiving Network are resized into $512 \times 7 \times 7$ and $1280 \times 7 \times 7$ respectively.

In Absolute-Attribute Interacting Network, all feature maps sent in are resized into $512 \times 7 \times 7$ through multiple conv layers with 1×1 kernel and then, they are concatenated and sent to channel attention block. In the channel attention block, the concatenation of feature maps is resized into two feature vectors through an Average Pooling Layer and Max Pooling Layer. Then we use them to calculate two channel attention vectors through one MLP and get the final channel attention vectors by element-wise summation. The process of the channel attention block can be formulated as follows:

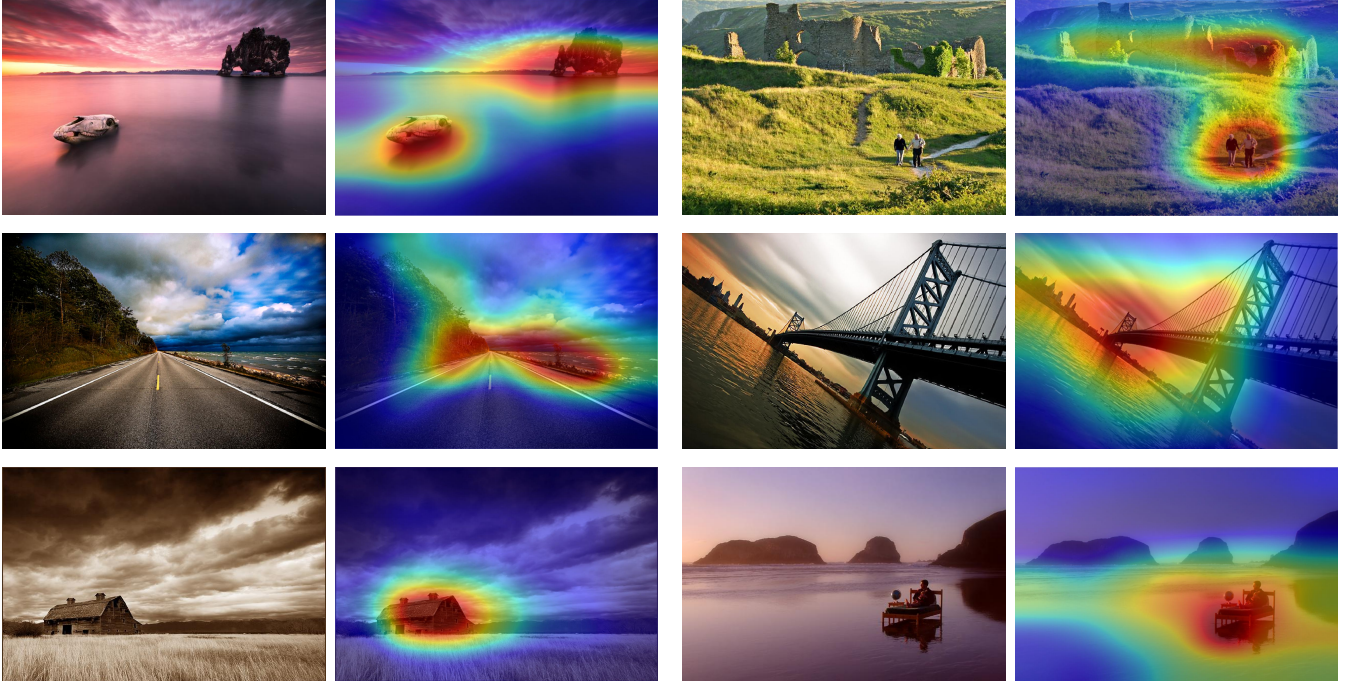


Fig. A2. More visualization results about composition attribute.

$$h = \sigma(MLP(f_1(c)) + MLP(f_2(c))) \odot c, \quad (5)$$

where c denotes the concatenation of absolute-attribute features and generic aesthetic feature before the channel attention block, and f_1 and f_2 denote the Max Pooling and Average Pooling. The MLP used is the same.

After that, we get out the absolute-attribute features and convert them into feature vectors with the size of $512 \times 1 \times 1$ via an Average Pooling Layer.

In the final feature fusion, we use the bilinear fusion [11] to fuse the overall attribute feature and generic aesthetic feature, its formulation can be set as follows:

$$\hat{p} = W_1 y_1 + W_2 y_2 + y_1^T W_3 y_2 + b, \quad (6)$$

where y_1 and y_2 denote the concatenation of all absolute attribute feature vectors and generic aesthetics feature vector respectively. W_1 , W_2 , and W_3 denote the learnable parameters and b is a real number. \hat{p} represents the output of the model.

C. MORE DETAILS AND EXPERIMENTS OF RELATIVE-RELATION LOSS

The introduced Relative-Relation Loss is implemented on the triplet loss [50]. Referring to the derivation in [37], in the condition of $g_i > g_j > g_k$, we want $|p_i - p_j| - |p_i - p_k| + margin \leq 0$, and since in a hypothetically perfect prediction environment, the predicted results can be set as the

ground truth, so, the inequality can be converted into $g_k - g_j + margin \leq 0$, thus the margin can be set as the upper limit $g_j - g_k$. By the same process, the margin can be set as $g_k - g_j$ in the condition of $g_i < g_j < g_k$. Thus, the margin of the used triplet loss is set as $|g_j - g_k|$.

For the balancing coefficient λ of the Relative-Relation Loss, we conduct more experiments about it on TAD66K dataset, and their results are shown in table A1.

Table A1. Results with different balancing coefficient of Relative-Relation Loss.

Balancing Coefficient λ	PLCC \uparrow	SRCC \uparrow
0.01	0.537	0.512
0.05	0.540	0.515
0.1	0.534	0.509
0.5	0.528	0.506

D. DATASETS AND EVALUATION METRICS

Datasets. Our experiments are mainly carried out on TAD66K [6] and AVA [45].

TAD66K dataset[6] is a newly proposed aesthetic assessment dataset and contains 66327 images with at least 1200 valid annotations for each image, which is more than any other aesthetic assessment dataset at present. Moreover, mea-

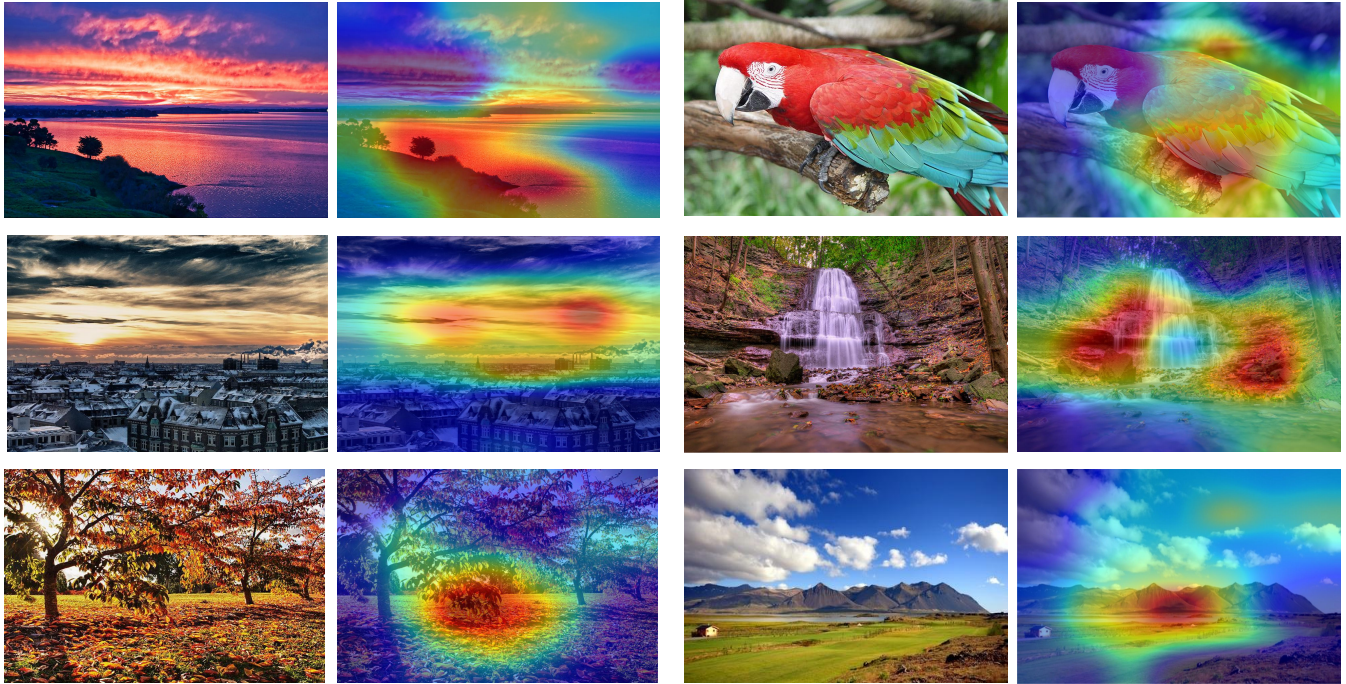


Fig. A3. More visualization results about color attribute.

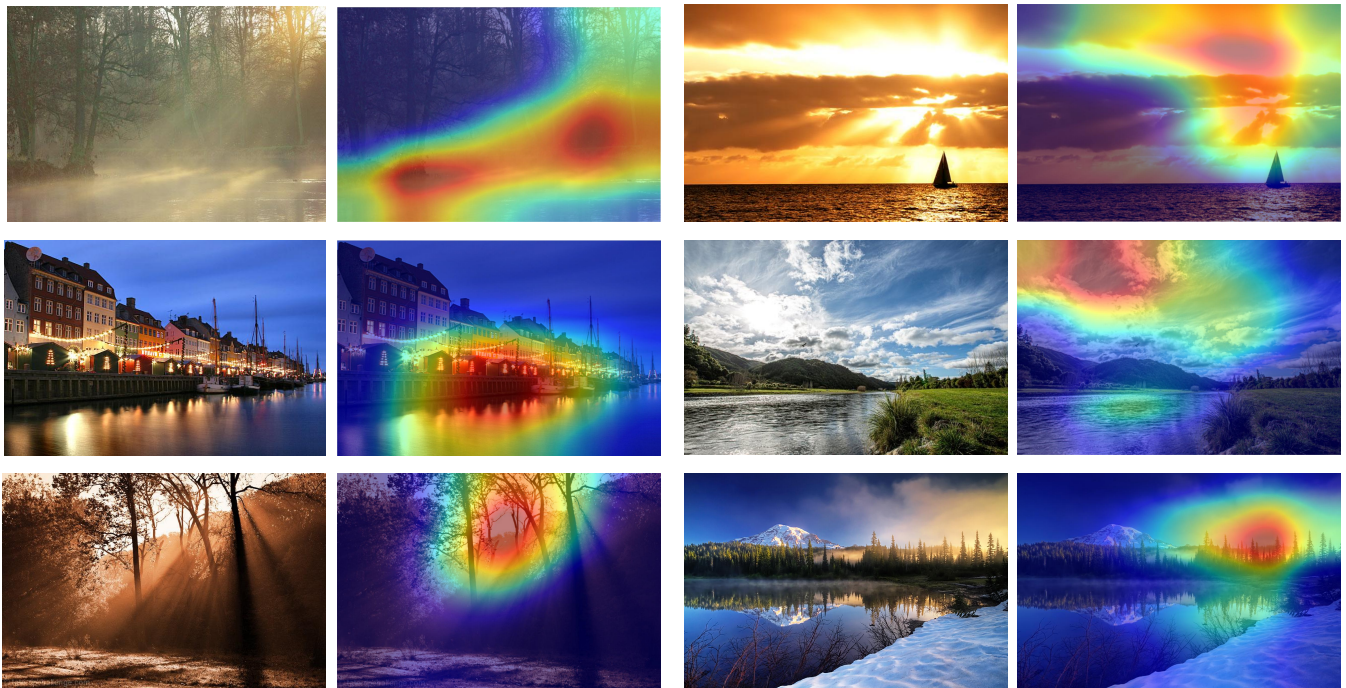


Fig. A4. More visualization results about exposure attribute.

sures are taken to effectively alleviate the problem of long-tailed distribution that exists in other aesthetic evaluation datasets. Since the accuracy and universality of the labels, we primarily conduct further experiments on the TAD66k

dataset.

AVA dataset[45] contains more than 255,000 images, each of which is voted on by 78-549 viewers with a voting score ranging from 1 to 10. The data partitioning is set up as in

the previous work [45, 6]. The score threshold is set as 5.0, classifying images with an average aesthetic score above 5.0 as high aesthetic quality and images with an average aesthetic score below 5.0 as low aesthetic quality.

Evaluation Metrics. In the evaluation phase, Pearson Linear Correlation Coefficient (PLCC) and Spearman's Rank Correlation Coefficient (SRCC) are used to evaluate the image scores predicted by the model. They are metrics used to measure the correlation between predicted scores and ground truth. The higher they are, the better the model performs. Specifically, an accuracy metric is used to evaluate the models' ability to classify high and low aesthetic quality on the AVA dataset. In addition, the MSE loss and EMD loss on test sets are also included in the evaluation metrics on TAD66K and AVA respectively to assess the model's performance.

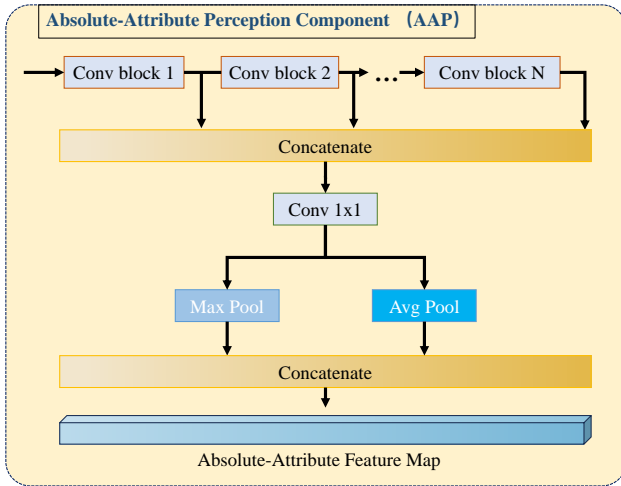


Fig. A5. Corresponding AAP structure for ‘w/o cnn’ setting.

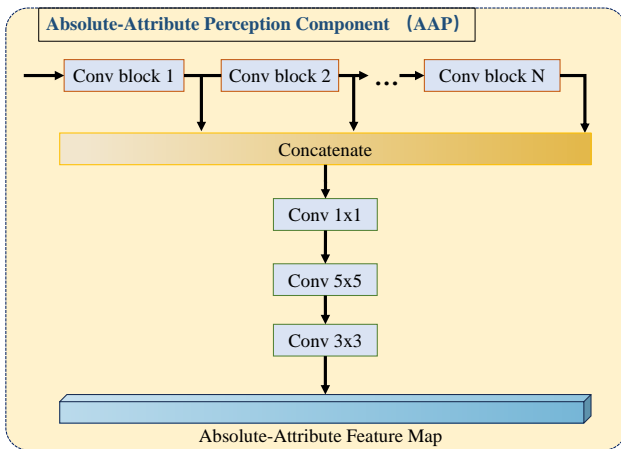


Fig. A6. Corresponding AAP structure for ‘w/o pool’ setting.



Fig. A7. Examples of changing the aesthetics attributes of the images. The scores below each images are their aesthetics scores predicting by our model.

E. MORE VISUALIZATION RESULTS

As shown in fig. A2, fig. A3, fig. A4, we show more comprehensive visualization results about different absolute-attributes extractors. In fig. A2, when faced with more diverse composition types, our composition attribute extractor is still able to focus on the areas that influence the composition of the image. In fig. A3, our color attribute extractor focuses on colors in the image as much as possible, thus extracting more comprehensive color information. In fig. A4, it can be seen that the areas about light information which will significantly influence the image’s exposure level and also has a significant impact on the aesthetics of the image have also received more attention.

F. MORE DETAILS OF THE ABLATION STUDY OF AAP

In the main text, we present the ablation experimental results of AAP with different structures. Among them, ‘w/o cnn’ and ‘w/o pool’ respectively represent two situations where pool layer and cnn layer are only applied on the connected feature map, and their specific structures are shown in fig. A5 and fig. A6.

G. SOME EXAMPLES OF THE CHANGE OF AESTHETICS SCORES AFTER CHANGING AESTHETICS ATTRIBUTES.

In this section, we attempt to change some aesthetic properties of the image, such as image brightness, color saturation, and composition. As shown in fig. A7, reasonably modifying the aesthetic attributes of an image can effectively improve its visual appeal. It also indicates that a good aesthetic evaluation model can guide the image modification in the real life.